# Numerical methods for plasma sheaths

Valentin Ayot[*], Mehdi Badsi, Yann Barsamian, Anaïs Crestetto,
Nicolas Crouseilles, Michel Mehrenberger, Averil Prost[†], Christian Tayou-Fotso[‡]

*Centre de Calcul Intensif d'Aix-Marseille is acknowledged for granting access to its high performance computing resources*

**Abstract**

This article is a report of the CEMRACS 2022 project, called HIVLASHEA, standing for "**Hi**gh order methods for **Vla**sov-Poisson models for **shea**ths". A two-species Vlasov-Poisson model is described together with some numerical simulations, permitting to exhibit the formation of a plasma sheath. The numerical simulations are performed with two different methods: a first order classical finite difference scheme and a high order semi-Lagrangian scheme with Strang splitting; for the latter one, the implementation of (non-periodic) boundary conditions is discussed. The codes are first evaluated on a one-species case, where a analytical solution is known. For the two-species case, mesh refinement and cross comparisons of the two methods are performed.

## 1 Introduction

Plasmas are neutral at the equilibrium in a sufficiently large domain. However, near a boundary, a charge imbalance may be observed in a thin layer called *sheath*. This phenomenon stems from the interaction of ions and electron with the boundary media (a cold metallic wall, for instance). Both species will be absorbed by the wall, but with a rate proportional to their speed. Since the electrons are moving faster than the ions, a positively charged layer (the *Debye sheath*) forms near the boundary.

Plasma sheaths are particularly challenging to simulate, as we have to deal with different scales. We refer to [BMG$^+$] for a recent work on the subject. This study is a follow-up of [BMN]. In the latter work, we studied the behavior of the numerical solution of the Vlasov equation, initialized with a sheath equilibrium. In this work, our purpose is to investigate numerically the formation of a sheath, when we include ionization in the model.

In Section 2, we introduce the corresponding system. The numerical methods are described in Section 3 and numerical results are given in Section 4.

## 2 Plasma sheaths

**The model** Let $t \in \mathbb{R}^+$ denote the time variable, $x \in [-1, 1]$ denote the spatial variable in a normalized one-dimensional domain, and $v \in \mathbb{R}$ denote the speed variable. The distribution of species is described through their density in the phase space, denoted by $f_i : (t, x, v) \in \mathbb{R}^+ \times [-1, 1] \times \mathbb{R} \mapsto \mathbb{R}$ for the ions, and

[*]Institut de Mathématiques, CNRS, UMR 5251, Université de Bordeaux, F-33405 Talence, France. valentin.ayot@u-bordeaux.fr

[†]INSA de Rouen, LMI (EA 3226 - FR CNRS 3335), 685 Avenue de l'Université, 76801 St Etienne du Rouvray cedex, France. averil.prost@insa-rouen.fr

[‡]Labo. J. A. Dieudonné, UMR 6621, Université Nice-Sophia Antipolis, Parc Valrose, F-06108 Nice cedex 02, France. christian.tayou-fotso@unice.fr

$f_e : (t, x, v) \in \mathbb{R}^+ \times [-1, 1] \times \mathbb{R} \mapsto \mathbb{R}$ for the electrons. To these kinetic quantities, we add the spatial densities $n_{i,e}$ and currents $J_{i,e}$, defined by

$$n_{i,e}(t, x) \coloneqq \int_{v \in \mathbb{R}} f_{i,e}(t, x, v) dv, \quad \text{and} \quad J_{i,e}(t, x) \coloneqq \int_{v \in \mathbb{R}} v f_{i,e}(t, x, v) dv. \tag{2.1}$$

In the sequel, we will denote $n(t, x) \coloneqq n_i(t, x) - n_e(t, x)$, and $J(t, x) \coloneqq J_i(t, x) - J_e(t, x)$.

The evolution of the densities is modelled by the Vlasov-Poisson equations. Let $\varphi : \mathbb{R}^+ \times [-1, 1] \mapsto \mathbb{R}$ denote the electric potential. Then

$$\begin{cases} \partial_t f_i + v \partial_x f_i - \partial_x \varphi \, \partial_v f_i = \nu f_e & (t, x, v) \in \mathbb{R}_*^+ \times ]-1, 1[ \times \mathbb{R}, \quad (2.2a) \\ \partial_t f_e + v \partial_x f_e + \dfrac{\partial_x \varphi}{\mu} \, \partial_v f_e = 0 & (t, x, v) \in \mathbb{R}_*^+ \times ]-1, 1[ \times \mathbb{R}, \quad (2.2b) \\ -\lambda^2 \partial_{xx}^2 \varphi = n(t, x) & (t, x) \in \mathbb{R}^+ \times ]-1, 1[. \quad (2.2c) \end{cases}$$

The physical parameters $\nu$, $\mu$ and $\lambda$ have the following meaning:

- $\nu \geqslant 0$ is the ionization frequency. It describes the rate of creation of ions in presence of electrons.
- $\mu \coloneqq m_e / m_i$ is the mass ratio between electrons and ions.
- $\lambda > 0$ is the Debye length.

In the sequel, we may use the electric field $E(t, x) \coloneqq -\partial_x \varphi(t, x)$ in place of the potential. Then, the second-order Poisson equation rewrites as

$$\lambda^2 \partial_x E(t, x) = n(t, x) \qquad (t, x) \in \mathbb{R}^+ \times ]-1, 1[. \tag{2.3}$$

**Remark 2.1.** *To reduce the notations, we will use $f_s$, $s \in \{i, e\}$ to denote both the electronic and ionic distributions. The advection equations* (2.2a) *and* (2.2b) *rewrite*

$$\partial f_s + v \partial_x f_s - c_s \partial_x \varphi \partial_v f_s = S_s,$$

*with the speed coefficients $c_s$ and source terms $S_s$ defined as*

$$c_i \coloneqq 1, \quad c_e \coloneqq -\frac{1}{\mu}, \quad S_i \coloneqq \nu f_e, \quad S_e \coloneqq 0.$$

The densities $f_i$ and $f_e$ are subject to initial and boundary conditions, given by

$$\begin{cases} f_s(0, x, v) \coloneqq f_s^0(x, v) & (x, v) \in ]-1, 1[ \times \mathbb{R}, \quad (2.4a) \\ f_s(t, x = \pm 1, \pm v < 0) \coloneqq 0 & t \in \mathbb{R}_*^+. \quad (2.4b) \end{cases}$$

The homogeneous boundary condition (2.4b) stems from the non-emitting wall model: the boundary absorbs particles without any reflection.

To completely describe the model, we still need to provide boundary conditions for the Poisson problem (2.2c). A first one is given by the choice of a reference potential

$$\varphi(t, 0) = 0 \qquad \forall t \in \mathbb{R}^+. \tag{2.5}$$

To derive a second boundary condition, we introduce a fundamental symmetry assumption.

**Symmetry** We will look for *symmetric solutions* satisfying

$$\varphi(t,x) = \varphi(t,-x) \qquad (t,x) \in \mathbb{R}^+ \times [-1,1]. \tag{2.6}$$

By derivation with respect to $x \in ]-1,1[$, we immediately obtain

$$\partial_x \varphi(t,x) = -\partial_x \varphi(t,-x), \quad \text{i.e.} \quad E(t,x) = -E(t,-x).$$

In particular, the electric field vanishes at $x = 0$, and the Neumann boundary condition

$$\partial_x \varphi(t,0) = 0 \quad \text{or equivalently} \quad E(t,0) = 0 \tag{2.7}$$

may be used (with (2.5)) to close the Poisson equation (2.2c).

Let us notice that the advection equations (2.2a) and (2.2b) are driven by the vector fields

$$(t,x,v) \to (1, v, E(t,x)) =: V_i(t,x,v) \quad \text{and} \quad (t,x,v) \to (1, v, -E(t,x)/\mu) =: V_e(t,x,v).$$

Both these fields satisfy the radial symmetry $V_s(t,x,v) = V_s(t,-x,-v)$. In consequence, if we assume that $f_s^0(x,v) = f_s^0(-x,-v)$, the solutions $f_s(t,x,v)$ will be radially symmetric around $(t,0,0)$, i.e.

$$f_i(t,x,v) = f_i(t,-x,-v) \quad \text{and} \quad f_e(t,x,v) = f_e(t,-x,-v) \quad \forall (t,x,v) \in \mathbb{R}^+ \times [-1,1] \times \mathbb{R}.$$

In particular, we have

$$\begin{aligned} n_s(t,x) &= \int_{v\in\mathbb{R}} f_s(t,x,v)dv = \int_{w\in\mathbb{R}} f_s(t,x,-w)dw = \int_{w\in\mathbb{R}} f_s(t,-x,w)dw = n_s(t,-x), \quad \text{and} \\ J_s(t,x) &= \int_{v\in\mathbb{R}} v f_s(t,x,v)dv = -\int_{w\in\mathbb{R}} w f_s(t,x,-w)dw = -\int_{w\in\mathbb{R}} w f_s(t,-x,w)dw = -J_s(t,-x). \end{aligned}$$

**Remark 2.2** (Additional symmetry of $f_e$)**.** *Notice that the function $f : (t,x,v) \to f_e(t,x,v) - f_e(t,x,-v)$ satisfies the linear equation*

$$0 = \partial_t f(t,x,v) + v\partial_x f(t,x,v) - \frac{E(t,x)}{\mu}\partial_v f(t,x,v).$$

*The boundary condition* (2.4b) *gives $f(t,\pm 1, \pm v < 0) = 0$. If, in addition, we assume that the initial condition $f_e^0$ satisfies $f_e^0(x,v) - f_e^0(x,-v) = 0$, then we obtain*

$$f_e(t,x,v) = f_e(t,x,-v) \quad \forall (t,x,v) \in \mathbb{R}^+ \times [-1,1] \times \mathbb{R}. \tag{2.8}$$

**Deriving a boundary condition at $x = \pm 1$** The centered Neumann condition (2.7) enforces continuity of $\partial_x \varphi$ at $x = 0$. We may avoid this constraint by deriving another Neumann condition, given on the boundary $x = \pm 1$.

First, we derive with respect to time the Poisson equation (2.2c)

$$-\partial_t(\lambda^2 \partial_{xx}^2 \varphi) = \partial_t n,$$

and considering the difference between the $v$-integration of the Vlasov equations (2.2a) and (2.2b) gives

$$\partial_t n = \nu n_e - \partial_x J,$$

so that, using $E = -\partial_x \varphi$, we get

$$\partial_x(\lambda^2 \partial_t E + J) = \nu n_e, \quad \forall x \in ]-1,1[.$$

Integrating now in space leads to

$$\lambda^2 \partial_t E(t,1) + J(t,1) = \lambda^2 \partial_t E(t,-1) + J(t,-1) + \nu \int_{-1}^{1} n_e(t,x)dx, \tag{2.9}$$

and using the symmetries $E(t,1) = -E(t,-1)$ and $J(t,1) = -J(t,-1)$, it comes

$$\lambda^2 \partial_t E(t,\pm 1) + J(t,\pm 1) = \pm \frac{\nu}{2} \int_{-1}^{1} n_e(t,x)dx. \tag{2.10}$$

Time integration gives a condition of the form $\partial_x \varphi(t,\pm 1) = C_\pm(t)$, where

$$C_\pm(t) \coloneqq \partial_x \varphi(0,\pm 1) + \frac{1}{\lambda^2} \int_0^t J(s,\pm 1)ds \mp \frac{\nu}{2\lambda^2} \int_0^t \int_{-1}^{1} n_e(s,x)dxds. \tag{2.11}$$

# 3 Numerical methods

## 3.1 Poisson equation

The Poisson problem is solved with integral representations of the variable $E$.

First, we consider the centered Neumann boundary condition (2.7). Then, integrating the Poisson problem (2.3) over $[0,x]$ yields

$$E(t,x) = 0 + \int_0^x n(t,y)dy = \int_0^x \int_{v\in\mathbb{R}} [f_i(t,y,v) - f_e(t,y,v)]dvdy. \tag{3.1}$$

Let us now consider the boundary condition (2.10). The spacial domain $[-1,1]$ is split into its positive and negative part, and integrating (2.3) gives

$$E(t,x) = \begin{cases} E(t,\ \ 1) - \int_x^1 \ n(t,y)dy = -C_+(t) - \int_x^1 \ \int_{v\in\mathbb{R}} [f_i(t,y,v) - f_e(t,y,v)]dvdy & x \in [0,1] \\ E(t,-1) + \int_{-1}^x n(t,y)dy = -C_-(t) + \int_{-1}^x \int_{v\in\mathbb{R}} [f_i(t,y,v) - f_e(t,y,v)]dvdy & x \in [-1,0[ \end{cases} \tag{3.2}$$

Note that here, the electric field may "jump" at $x = 0$. Both expressions may be approximated by quadrature formulas.

## 3.2 Finite Differences (FD)

Define a numerical computation domain $\Omega \coloneqq [-1,1] \times [-\overline{V}, \overline{V}]$, with a large enough maximum speed $\overline{V}$. Let $(x_j, v_k)_{k\in[\![0,K]\!]}^{j\in[\![0,J]\!]}$ be a cartesian grid of $\Omega$ of step $(\Delta x, \Delta v)$. We discretize the advection equations on the subgrid $(x_j, v_k)_{k\in[\![1,K-1]\!]}^{j\in[\![1,J-1]\!]}$ by an explicit Euler scheme in time, and the upwind scheme in space:

$$\frac{f_{s,j,k}^{n+1} - f_{s,j,k}^n}{\Delta t} + D_{j,k}^- f_s^n \begin{pmatrix} v_k \\ c_s E_j^n \end{pmatrix}_+ + D_{j,k}^+ f_s^n \begin{pmatrix} v_k \\ c_s E_j^n \end{pmatrix}_- = S_{s,j,k}^n, \tag{3.3}$$

where $a_+ = \max(a,0)$ and $a_- = \min(a,0)$ are respectively the pointwise positive and negative parts, and the decentered discrete differences are defined as

$$D_{j,k}^\pm f \coloneqq \pm \left( \frac{f_{j\pm1,k} - f_{j,k}}{\Delta x}, \frac{f_{j,k\pm1} - f_{j,k}}{\Delta v} \right).$$

The values of $f_{s,j,k}^n$ on the boundary are taken as follows:

– the boundary condition (2.4b) yields $f_{s,j,k}^n = 0$ whenever $x_j = -1, v_k > 0$ or $x_j = 1, v_k < 0$.

– It is considered that $\overline{V}$ is large enough to take the values on the speed boundary $v_k = \pm\overline{V}$ equal to 0.

– The remaining values $f^n_{s,j,k}$, $x_j = -1, -\overline{V} < v_k \leqslant 0$ or $x_j = 1, 0 \leqslant v_k < \overline{V}$ may be computed using the scheme (3.3), since the sign of the speed allows to use only inner points.

The upwind scheme is known to be diffusive, and stable under the CFL condition

$$1 - \max_k |v_k| \frac{\Delta t}{\Delta x} - |c_s| \max_j |E^n_j| \frac{\Delta t}{\Delta v} \geqslant 0 \quad \forall s \in \{i, e\} \text{ and } n \in [\![1, N]\!].$$

Given $\Delta x$ and $\Delta v$, we deduce a sufficiently small value of $\Delta t$ with the bound

$$\Delta t \leqslant \min\left(\frac{\Delta x}{\overline{V}}, \min(1, \mu)\frac{\Delta v}{E_{\max}}\right), \quad E_{\max} > 0 \text{ postulated } \textit{a priori}.$$

### 3.3 Semi-Lagrangian (SL)

The full model (2.2) nicely lends itself to approximation by time splitting. Indeed, consider the following Strang splitting decomposition.

$$\begin{array}{ll}
\dfrac{\Delta t}{2} & \begin{cases} \partial_t f_s + v\partial_x f_s = 0 & \text{Linear advection along } x, \\ \lambda^2 \partial_x E = n_i - n_e & \text{Poisson problem,} \end{cases} \\
\dfrac{\Delta t}{2} & \partial_t f_i = \nu f_e \qquad \text{Ionization,} \\
\Delta t & \partial_t f_s + c_s E \partial_v f_s = 0 \quad \text{Linear advection along } v, \\
\dfrac{\Delta t}{2} & \partial_t f_i = \nu f_e \qquad \text{Ionization,} \\
\dfrac{\Delta t}{2} & \begin{cases} \lambda^2 \partial_x E = n_i - n_e & \text{Poisson problem,} \\ \partial_t f_s + v\partial_x f_s = 0 & \text{Linear advection along } x. \end{cases}
\end{array}$$

Each of the splitting step may be solved exactly. Indeed, the Poisson problems are solved by the integral representations (3.1) and (3.2). The ionization steps are pointwise ODE with time-independant source term, and are exactly solved by the explicit Euler scheme. Finally, notice that each advection is at constant speed with respect to the advection variable. This allows for the use of elementary 1D solvers.

**Numerical treatment of the boundaries** Let us focus on the elementary advection equation with constant speed $a > 0$

$$\partial_t f(t, x) + a\partial_x f(t, x) = 0, \quad f(t, -1) = 0, \quad \forall (t, x) \in \mathbb{R}^+_* \times ]-1, 1[.$$

Let $(x_j)_{j \in [\![0,J]\!]}$ be a space mesh of step $\Delta x \coloneqq 2/J$, and $(t_n)_{n \in [\![0,N]\!]}$ be a time mesh of step $\Delta t \coloneqq T/N$. We follow the work of [CL20], and consider a semi-Lagrangian scheme defined as

$$f^{n+1}_j = \text{Lagrange interpolation}\,(f^n, x_j - a\Delta t) \coloneqq \sum_{k=-d}^{d+1} f^n_{j_0+k} L_k(\alpha),$$

with $(L_k)_{k \in [\![-d, d+1]\!]}$ the Lagrange polynomes defined by $L_k(z) = \prod_{\ell=-d, \ell\neq k}^{d+1} \frac{z-k}{\ell-k}$ (which satisfy $L_k(\ell) = \delta_{k\ell}$ for $\ell \in [\![-d, d+1]\!]$), and $x_j - a\Delta t = x_{j_0} + \alpha\Delta x$, $j_0 \in \mathbb{Z}, \alpha \in [0, 1[$. The boundaries are treated as follows:

– the *inflow* side, corresponding to $x = -1$, relies on the analytical solution $f(t, x) = 0\ \forall x \leqslant at$. Whenever the scheme needs a value $f^n_j$ with $j < 0$, it may be exactly taken equal to 0.

– in the case $d > 0$, the Lagrange stencil may also need *outflow* values $f^n_j$ with $j > J$. Such values may be determined by polynomial extrapolation. Let $k_b \in \mathbb{N}$, and let $p$ be the unique polynomial of degree $k_b$ interpolating $(x_j, f^n_j)$ for $j \in [\![J - k_b, J]\!]$. The *outflow ghost points* will be defined by $f^n_j \coloneqq p(-1 + j\Delta x)\ \forall j > N$.

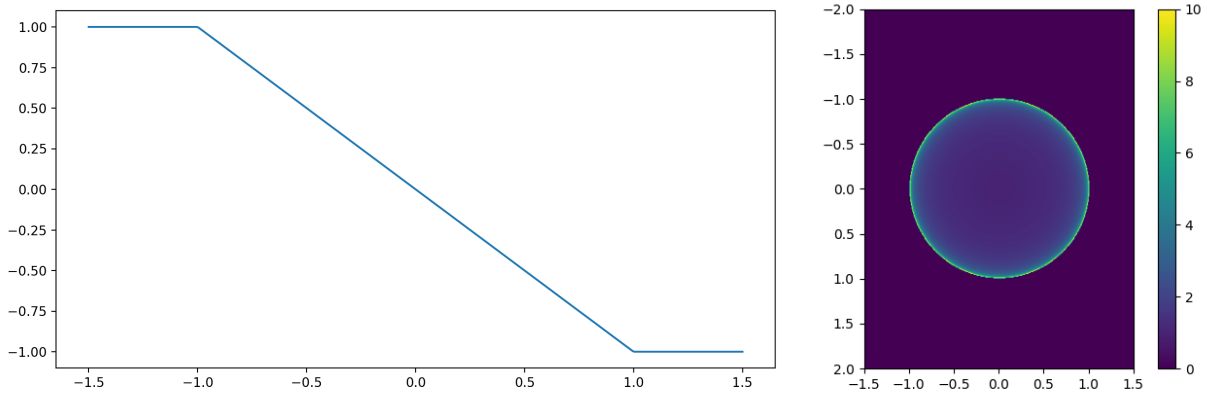


Figure 1: Malkov solutions (4.4) on $[-1.5, 1.5]$. Right: electric field $E$. Left: density $f$.

*The electric field is extended outside of $[-1, 1]$ by a constant. The density $f$ is represented in the domain $[-1.5, 1.5] \times [-2, 2]$, and truncated to 10.*

# 4 Numerical results

## 4.1 1-species validation test case

We rely on the work of [MK20] to provide an analytical solution in a 1-species case. Consider the simplified stationary model describing the density of particles $f = f(t, x, v)$, and the potential $\varphi = \varphi(t, x)$:

$$\begin{cases} \partial_t f + v\partial_x f - \partial_x \varphi \partial_v f = 0 & (t, x, v) \in \mathbb{R}_*^+ \times ]-1, 1[ \times \mathbb{R}, \quad (4.1a) \\ \partial_{xx}^2 \varphi = \displaystyle\int_{v \in \mathbb{R}} f dv & (t, x) \in \mathbb{R}^+ \times ]-1, 1[. \quad (4.1b) \end{cases}$$

The initial and boundary conditions are given by

$$\begin{cases} f(0, x, v) \coloneqq f^0(x, v), \quad f(t, x = \pm 1, \pm v < 0) = 0 & (4.2a) \\ \varphi(t, 0) = \partial_x \varphi(t, 0) = 0 & (4.2b) \end{cases}$$

This model may be seen as a particular case of the two-species Vlasov-Poisson (2.2), upon taking the following parameters:

$$f_i^0 \equiv 0, \quad \nu = 0, \quad \mu = -1, \quad \lambda = 1, \quad f_e^0 = f^0.$$

The reader may verify that (4.1) is solved in $\mathbb{R}^+ \times [-1, 1] \times \mathbb{R}$ by the following stationary couple:

$$f(t, x, v) \coloneqq \begin{cases} \frac{1}{\pi} \left(1 - x^2 - v^2\right)^{-1/2} & \text{if } x^2 + v^2 < 1 \\ 0 & \text{otherwise} \end{cases}, \quad \text{and} \quad \varphi(t, x) \coloneqq \frac{x^2}{2}. \quad (4.3)$$

It is numerically relevant to extend the Malkov solution (4.3) to spatial domains $x \in [-1 - \varepsilon, 1 + \varepsilon]$ by

$$f(t, x, v) \coloneqq \begin{cases} \frac{1}{\pi} \left(1 - x^2 - v^2\right)^{-1/2} & \text{if } x^2 + v^2 < 1 \\ 0 & \text{otherwise} \end{cases}, \quad \text{and} \quad \varphi(t, x) \coloneqq \begin{cases} x^2/2, & x < 1 \\ |x| - \frac{1}{2}, & x \geq 1 \end{cases} \quad (4.4)$$

Figure (1) illustrates the stationary solutions.
**For now, I don't reach order 1. Maybe bug?**

| Parameters | | | Errors | |
|---|---|---|---|---|
| $N_x$ | $N_v$ | $N_t$ | $L^\infty$ | $L^1$ |
| 100 | 2049 | 1281 | 8.59e-03 | 6.22e-03 |
| 200 | 2049 | 1281 | 1.22e-02 | 1.78e-02 |
| 400 | 2049 | 1281 | 6.22e-03 | 9.07e-03 |
| 800 | 2049 | 1281 | 7.13e-03 | 7.23e-03 |
| 100 | 4097 | 2561 | 5.65e-03 | 4.92e-03 |
| 200 | 4097 | 2561 | 3.88e-03 | 4.70e-03 |
| 400 | 4097 | 2561 | 4.08e-03 | 5.77e-03 |
| 800 | 4097 | 2561 | 2.39e-03 | 2.93e-03 |

Table 1: DF errors for Malkov test case.

| Parameters | | | Errors | |
|---|---|---|---|---|
| $N_x$ | $N_v$ | $N_t$ | $L^\infty$ | $L^1$ |
| 100 | 201 | 1000 | 1.30e-02 | 1.59e-03 |
| 200 | 401 | 1000 | 1.66e-02 | 1.88e-03 |
| 400 | 801 | 1000 | 1.88e-02 | 1.35e-03 |
| 800 | 1601 | 1000 | 6.15e-03 | 2.66e-04 |
| 100 | 101 | 100 | 3.19e-02 | 3.45e-03 |
| 200 | 201 | 200 | 2.77e-02 | 3.13e-03 |
| 400 | 401 | 400 | 6.49e-03 | 4.35e-04 |
| 800 | 801 | 800 | 1.51e-02 | 8.50e-04 |
| 1600 | 1601 | 1600 | 6.57e-03 | 2.50e-04 |
| 100 | 2049 | 10000 | 4.06e-03 | 4.62e-04 |
| 200 | 2049 | 10000 | 1.72e-02 | 1.40e-03 |
| 400 | 2049 | 10000 | 7.88e-03 | 3.90e-04 |
| 800 | 2049 | 10000 | 1.12e-02 | 5.37e-04 |
| 1000 | 201 | 5000 | 1.00e-02 | 3.32e-04 |
| 1000 | 401 | 5000 | 1.16e-02 | 5.48e-04 |
| 1000 | 801 | 5000 | 5.01e-03 | 1.72e-04 |
| 1000 | 1601 | 5000 | 6.34e-03 | 3.25e-04 |

Table 2: SL errors for Malkov test case.

## 4.2 Comparison between (SL) and (FD)

In the sequel, we use the following physical parameters:

$$\lambda = \frac{1}{2}, \quad \mu = \frac{1}{100}, \quad \text{and} \quad \nu = 20. \tag{4.5}$$

The initial conditions are chosen as the thermodynamic equilibrium in an infinite spatial domain, or in a domain with periodic condition. The densities are then given by

$$f_i^0(x,v) \coloneqq \frac{\exp\left(-\frac{v^2}{2}\right)}{\sqrt{2\pi}}, \quad \text{and} \quad f_e^0(x,v) \coloneqq \sqrt{\mu}\frac{\exp\left(-\mu\frac{v^2}{2}\right)}{\sqrt{2\pi}}.$$

In order to satisfy the boundary conditions, we multiply $f_{i,e}$ by a mask, defined as

$$\text{mask}(x,v) \coloneqq \frac{1}{2}\left(\tanh\left(\frac{x-(-0.8)}{0.1}\right) - \tanh\left(\frac{x-0.8}{0.1}\right)\right).$$

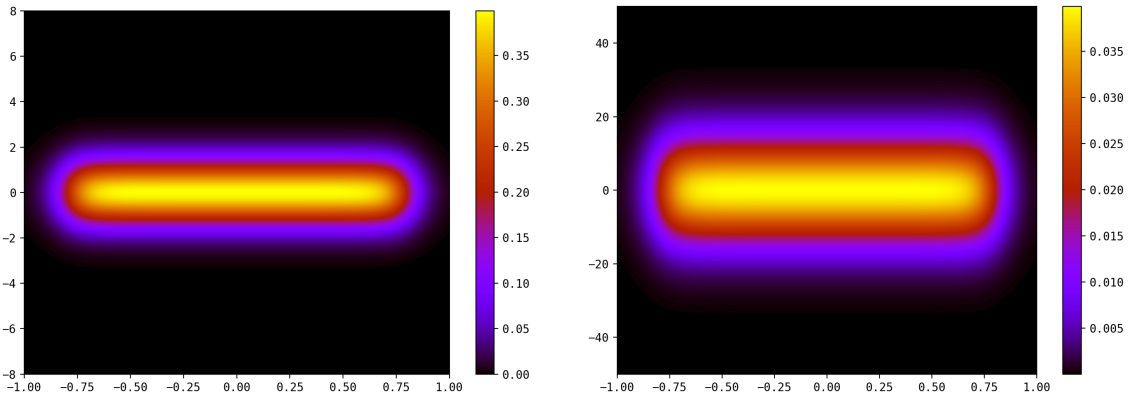

Figure 2: Initial conditions $f_i^0$ (left) and $f_e^0$ (right).

Figure (2) illustrates the resulting initial conditions.

**Short time** The simulations run over the spatial domain $x \in [-1, 1]$. The semi-Lagrangian code computes the electron velocities on $v_e \in [-50, 50]$, and ion velocities on $v_i \in [-8, 8]$. The finite differences code uses the same mesh for ions and electrons, chosen as $v \in [-50, 50]$. To simplify the comparison, visualisations of $f_i$ for (FD) are restricted to the coordinates $f_{i,j,k}$ such that $v_k \in [-8, 8]$.

Figure (3) illustrates the very short-time behaviour of both codes. At time $t = 0$, the initial conditions are chosen so that $E = \rho = 0$, corresponding to a neutral plasma. The initial velocity field is then given by $(v, 0)$, and we observe the shear of the initial conditions. The electric field conserve the same variations through both codes, with a difference in scale.

The same simulation at time $T = 0.1$ shows a greater divergence between both methods. The electric field does not have the same extremal values, and the comparison of $\rho$ reveals a difference of variations. The approximations of the ion density $f_i$ seem quite similar, but the shape of the electric density $f_e$ differs: the semi-lagrangian code produces sharper approximation and a more elongated profile.

**Long time** Now, we turn to the long-term simulations, with $T = 200$. Here, we free the semi-Lagrangian code from the artificial CFL condition imposed for fair comparisons. Figure (5) illustrates the behavior of both codes on long time, with parameters given by (4.5).

The finite difference code suffers from its diffusion, and the approximations of $f_i$ and $f_e$ are almost everywhere reduced to 0. The point $(x = 0, v = 0)$ stands out, since it is an equilibrium point: the value $f_e(t, 0, 0)$ is constant with respect to $t$ (both in the continuous model, and in the discrete model provided $(x = 0, v = 0)$ belongs to the mesh), and

$$\partial_t f_i(t, 0, 0) = f_e(t, 0, 0), \quad \text{so that} \quad f_i(t, 0, 0) = f_i(0, 0, 0) + t f_e(0, 0, 0).$$

This explains the results of fig. (5). The value $f^n_{e,j_0,k_0} \simeq f_e(T, 0, 0)$ is stationary, but the maximum of $f^n_e$ outside a small neighbourhood of $(x = 0, v = 0)$ is 0 at machine precision. The value $f^n_{i,j_0,k_0} \simeq f_i(T, 0, 0)$ is not taken into account in the colormap, since

$$\max_{j,k} f^n_{i,j,k} = f^n_{i,j_0,k_0} = 159.97581842617524, \quad \text{and} \quad \left| f^n_{i,j_0,k_0} - (f^0_{i,j_0,k_0} + T\nu f^0_{e,j_0,k_0}) \right| = 8.98 \times 10^{-9}.$$

At the opposite, the semi-Lagrangian scheme does not produce vanishing approximations.

**Numerical results for the SL code for different discretizations** We want here to compare the semi-Lagrangian code with different discretizations. We have here no exact solution at hand to validate the

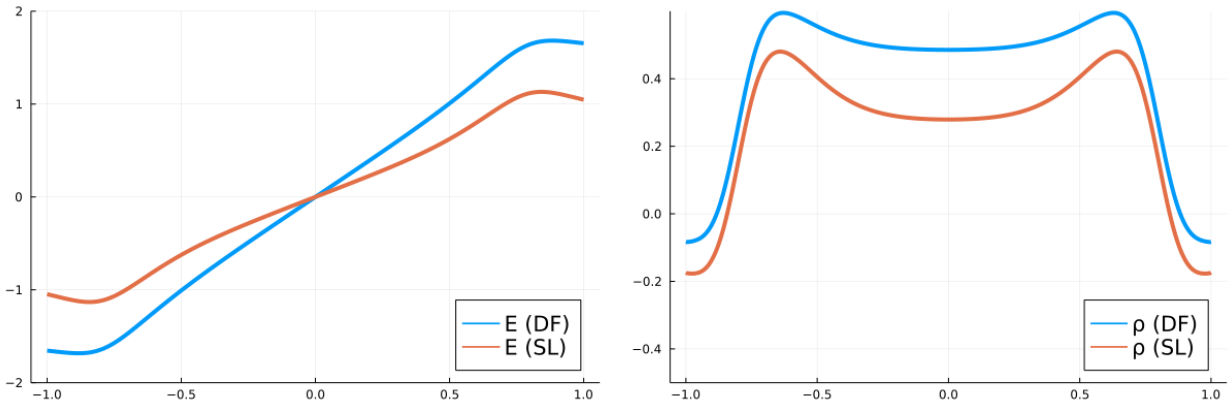


(a) Electric field (left) and density $\rho$ (right)

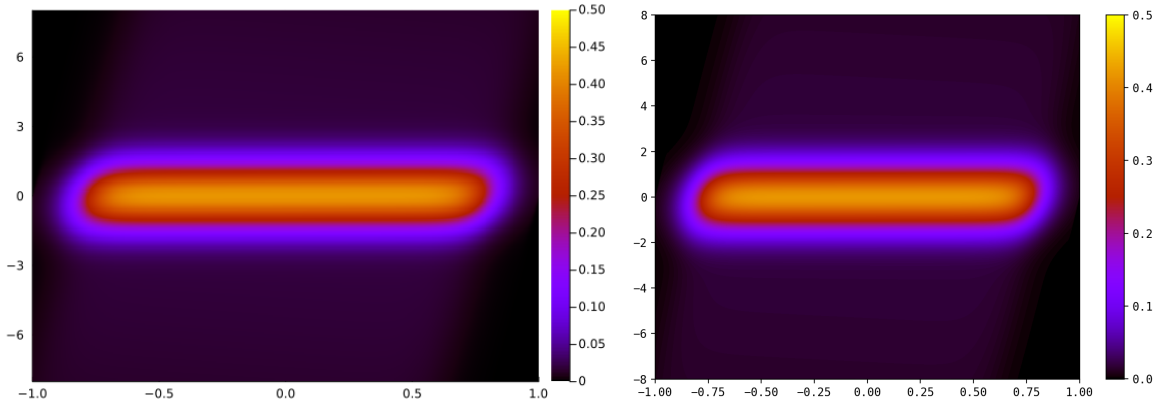

(b) Ion density

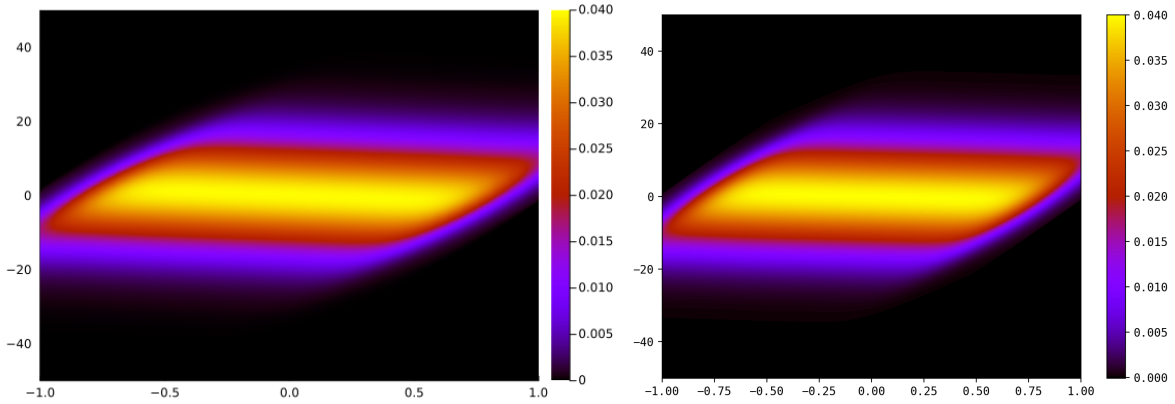

(c) Electron density

Figure 3: Comparison between finite differences (left) and semi-Lagrangian (right) at $T = 0.025$.

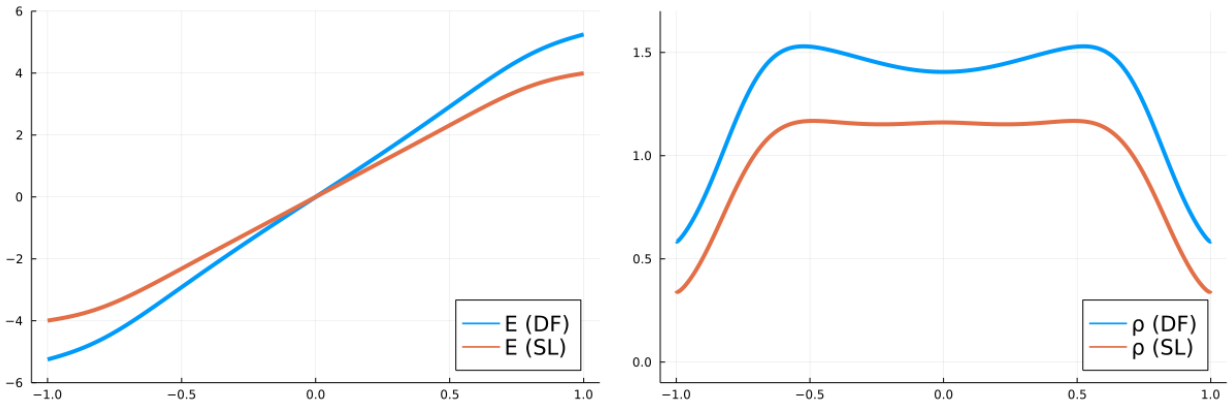


(a) Electric field (left) and density $\rho$ (right)

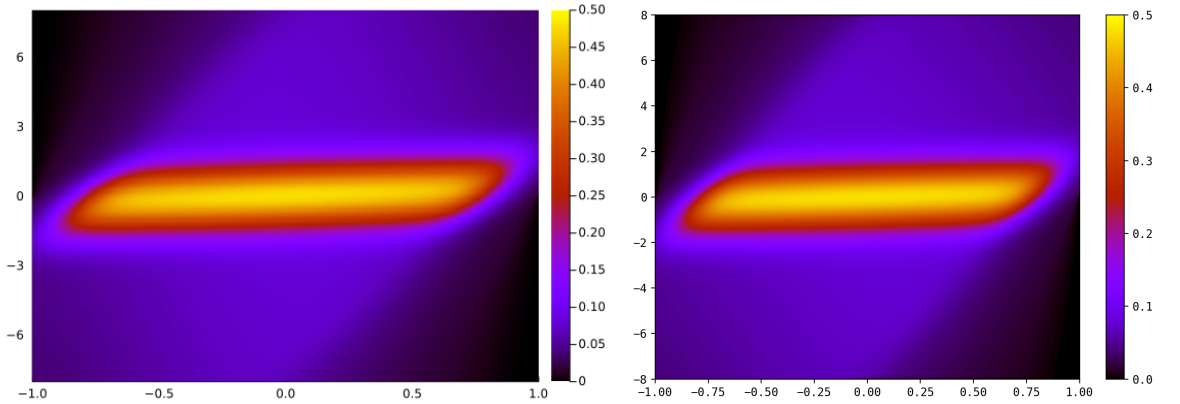

(b) Ion density

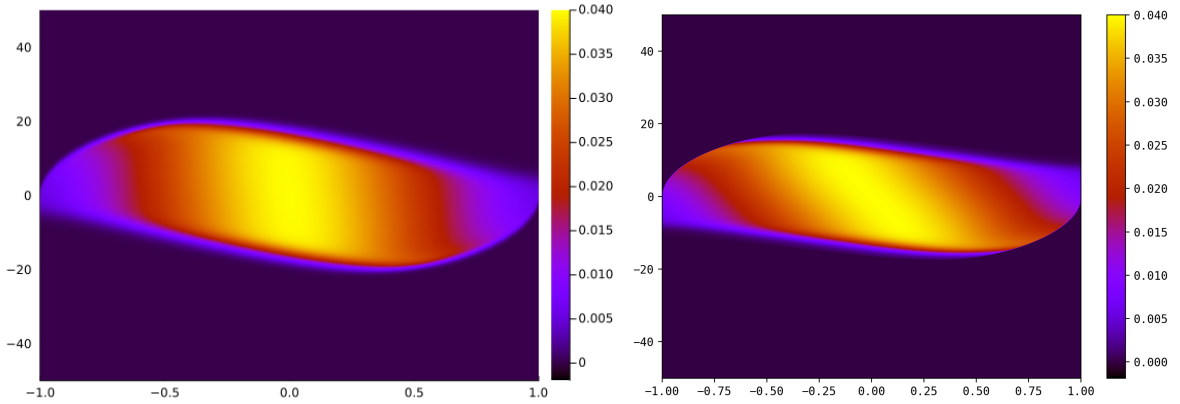

(c) Electron density

Figure 4: Comparison between finite differences (left) and semi-Lagrangian (right) at $T = 0.1$.

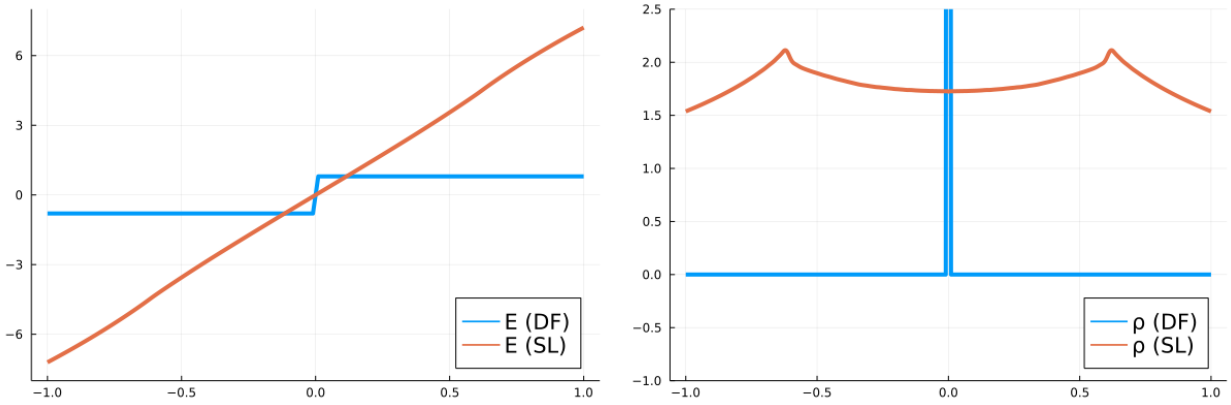


(a) Electric field (left) and density $\rho$ (right)

*The maximum of $\rho$ for the (DF) code is equal to 39.983965094090.*

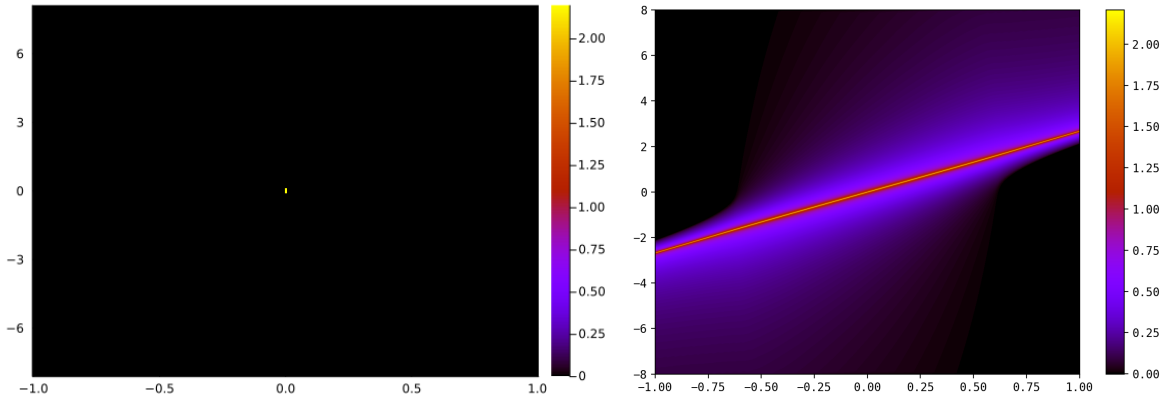

(b) Ion density

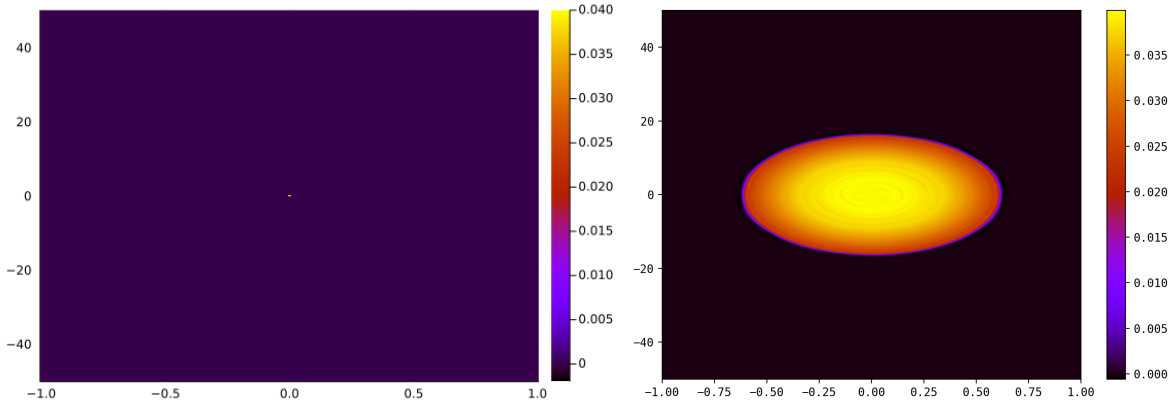

(c) Electron density

Figure 5: Comparison between finite differences (left) and semi-Lagrangian (right) at $T = 200$.

code; so we validate it by comparing the numerical parameters. We restrict here to final time $T = 20$ and look for "converged" numerical parameters. It is beneficial that the code is parallel (remap strategy of the selalib project[1]); in practice we do the simuations on a labtop or in the mesocentre of Marseille (16 cores for interactive mode and 32 cores for submitted jobs, which can be prone to delays, depending on the queue).

We choose to use a high number for the electron density, by taking $N_v = 8193$, and we study the change for $N_x$ and $N_{v_i}$, taking first $N_x = 256$ and $N_{v_i} = 2049$, and then taking $N_x = 1024$ and $N_{v_i} = 4097$. Numerical results are shown on Figure 6. We clearly see that the results are quite similar, with a more diffusive solution for the coarser mesh, which is encouraging.

On Figure 7, we study the validity of the time discretization, changing the value of $\Delta t$, which goes from $\Delta t = 0.00125$ to $\Delta t = 0.000125$. We again see that results are very similar, which is a good point.

We have used $d = 8$ with periodic boundary conditions for the interpolation in velocity, and $k_b = 1$ together with $d = 2$ for the spatial interpolation. Lagrange interpolation of degree 3 (that is, $d = 1$) is used for passing from the ion velocity mesh to the electron velocity mesh (which is needed for the ionization).

The ion density and the electric field seem not to change much; but the electron density is varying a lot and becomes more and more complex with respect to time, and filaments appear. Note that we have to take quite small time steps, as we have chosen $\mu = 1/100$, which makes the study more difficult, but it is nearer to more physically relevant parameters. We have chosen also a high number for $N_{v_e}$; this permits to better keep the symmetry, without imposing it a priori (which is in fact possible, by a symmetrization of $\rho$).

We remark also that the spatial interpolation does not lead to unstable results, which can occur sometimes when extrapolation is used (see [BMN]). We have used an odd number of points in order to prevent from having 0 as mesh points, which would lead to increase of the value at constant rate, in the ionization step.

The study of the numerical equilibrium and the study of the behavior of the ion densiity around $(0, 0)$ which is quite complex at equilibrium, are not tackled here and are out of the scope of this work.

# References


[BBC21] Mehdi Badsi, Christophe Berthon, and Anaïs Crestetto. A stable fixed point method for the numerical simulation of a kinetic collisional sheath. *Journal of Computational Physics*, 429:109990, March 2021.

[BMG+] Emily Bourne, Yann Munschy, Virginie Grandgirard, Michel Mehrenberger, and Philippe Ghendrih. Non-Uniform Splines for Semi-Lagrangian Kinetic Simulations of the Plasma Sheath. page 35.

[BMN] Mehdi Badsi, Michel Mehrenberger, and Laurent Navoret. Numerical stability of plasma sheath. page 16.

[CL20] Jean-François Coulombel and Frédéric Lagoutière. The Neumann numerical boundary condition for transport equations. *Kinetic & Related Models*, 13(1):1–32, 2020.

[GAB+16] V. Grandgirard, J. Abiteboul, J. Bigot, T. Cartier-Michaud, N. Crouseilles, G. Dif-Pradalier, Ch. Ehrlacher, D. Esteve, X. Garbet, Ph. Ghendrih, G. Latu, M. Mehrenberger, C. Norscini, Ch. Passeron, F. Rozar, Y. Sarazin, E. Sonnendrücker, A. Strugarek, and D. Zarzoso. A 5D gyrokinetic full- f global semi-Lagrangian code for flux-driven ion turbulence simulations. *Computer Physics Communications*, 207:35–68, October 2016.

[MK20] Evgeny A. Malkov and Alexey N. Kudryavtsev. Non-stationary Antonov self-gravitating layer: Analytics and numerics. *Monthly Notices of the Royal Astronomical Society*, 491:3952–3966, January 2020.


[1] `https://selalib.github.io/selalib.html`

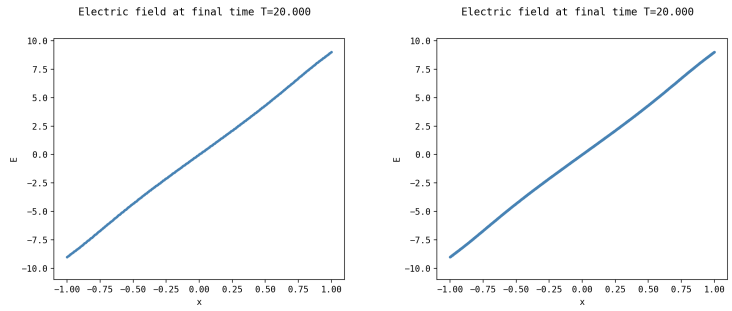


(a) Electric field

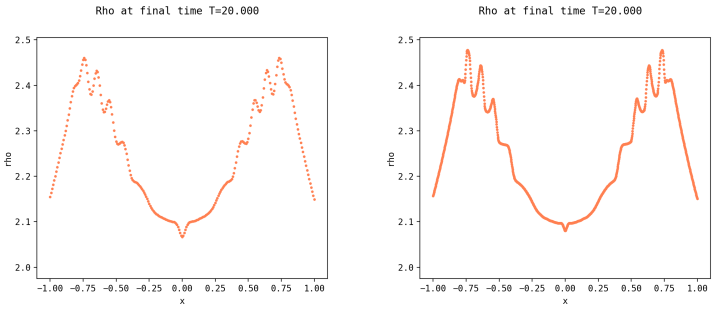


(b) Density $\rho$

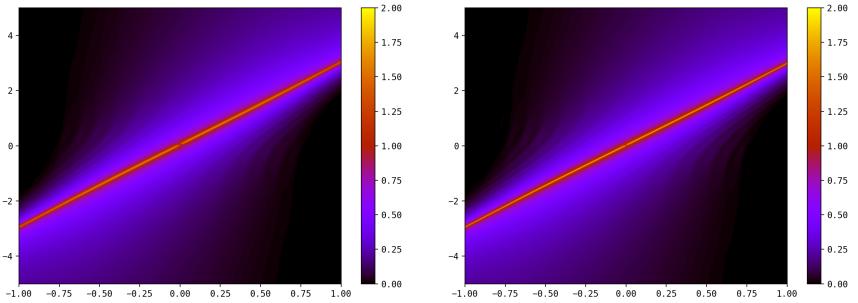

(c) Ion density

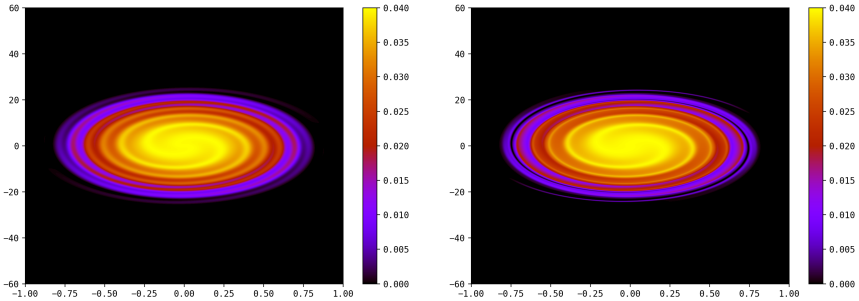

(d) Electron density

Figure 6: Comparison of semi-Lagrangian code for different discretizations. Run1: $N_x = 256$, $N_{v_i} = 2049$ (left); Run2: $N_x = 1024$, $N_{v_i} = 4097$ (right) at $T = 20$. Other numerical parameters are $N_{v_e} = 8193$ and $\Delta t = 0.00025$. We have used $[-60, 60]$ for $v_e$ and $[-50, 50]$ for $v_i$. The ion density is zoomed for $v_i \in [-4.5, 4.5]$

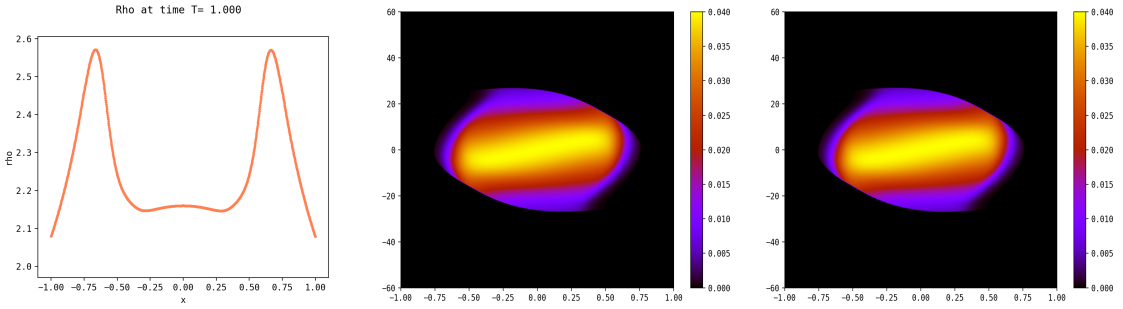


(a) $T = 1$

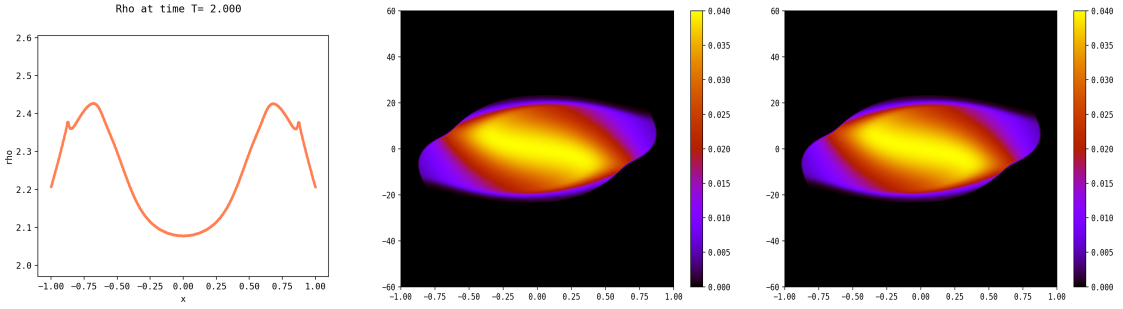


(b) $T = 2$

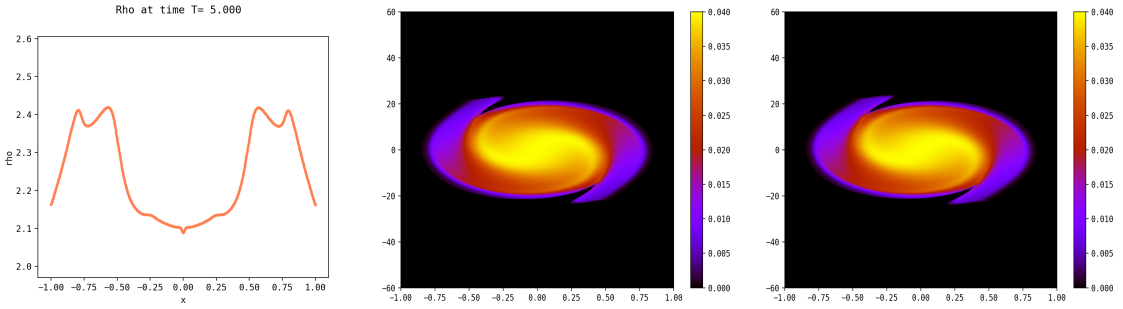


(c) $T = 5$

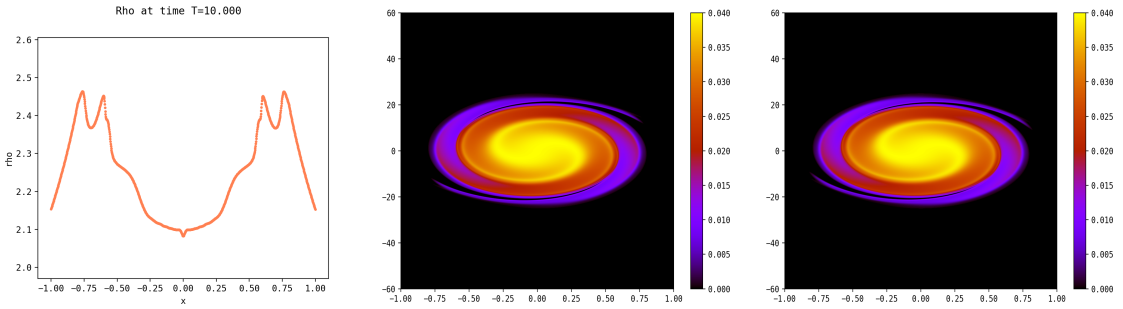


(d) $T = 10$

Figure 7: Density $\rho$ (left) and electron density (middle) for time $T \in \{1, 2, 5, 10\}$ with Run2; electron density is also given, by changing $\Delta t$ to 0.000025 (right)